

Fermi-LAT Discovery of Extended Gamma-ray Emission in the Direction of Supernova Remnant W51C

A. A. Abdo^{2,3}, M. Ackermann⁴, M. Ajello⁴, L. Baldini⁵, J. Ballet⁶, G. Barbiellini^{7,8},
M. G. Baring⁹, D. Bastieri^{10,11}, B. M. Baughman¹², K. Bechtol⁴, R. Bellazzini⁵,
B. Berenji⁴, R. D. Blandford⁴, E. D. Bloom⁴, E. Bonamente^{13,14}, A. W. Borgland⁴,
A. Bouvier⁴, J. Bregeon⁵, A. Brez⁵, M. Brigida^{15,16}, P. Bruel¹⁷, T. H. Burnett¹⁸,
S. Buson¹¹, G. A. Caliandro^{15,16}, R. A. Cameron⁴, P. A. Caraveo¹⁹, J. M. Casandjian⁶,
C. Cecchi^{13,14}, Ö. Çelik^{20,21,22}, A. Chekhtman^{2,23}, C. C. Cheung²⁰, J. Chiang⁴,
S. Ciprini^{13,14}, R. Claus⁴, J. Cohen-Tanugi²⁴, L. R. Cominsky²⁵, J. Conrad^{26,27,28},
S. Cutini²⁹, C. D. Dermer², A. de Angelis³⁰, F. de Palma^{15,16}, S. W. Digel⁴, M. Dormody³¹,
E. do Couto e Silva⁴, P. S. Drell⁴, R. Dubois⁴, D. Dumora^{32,33}, C. Farnier²⁴, C. Favuzzi^{15,16},
S. J. Fegan¹⁷, W. B. Focke⁴, P. Fortin¹⁷, M. Frailis³⁰, Y. Fukazawa³⁴, S. Funk^{4,1},
P. Fusco^{15,16}, F. Gargano¹⁶, D. Gasparrini²⁹, N. Gehrels^{20,35}, S. Germani^{13,14}, G. Giavitto³⁶,
B. Giebels¹⁷, N. Giglietto^{15,16}, F. Giordano^{15,16}, T. Glanzman⁴, G. Godfrey⁴, I. A. Grenier⁶,
M.-H. Grondin^{32,33}, J. E. Grove², L. Guillemot^{32,33}, S. Guiriec³⁷, Y. Hanabata³⁴,
A. K. Harding²⁰, M. Hayashida⁴, E. Hays²⁰, R. E. Hughes¹², M. S. Jackson^{26,27,38},
G. Jóhannesson⁴, A. S. Johnson⁴, T. J. Johnson^{20,35}, W. N. Johnson², T. Kamae⁴,
H. Katagiri³⁴, J. Kataoka^{39,40}, J. Katsuta^{41,42}, N. Kawai^{39,43}, M. Kerr¹⁸, J. Knödseder⁴⁴,
M. L. Kocian⁴, M. Kuss⁵, J. Lande⁴, L. Latronico⁵, M. Lemoine-Goumard^{32,33}, F. Longo^{7,8},
F. Loparco^{15,16}, B. Lott^{32,33}, M. N. Lovellette², P. Lubrano^{13,14}, A. Makeev^{2,23},
M. N. Mazziotta¹⁶, J. E. McEnery²⁰, C. Meurer^{26,27}, P. F. Michelson⁴, W. Mitthumsiri⁴,
T. Mizuno³⁴, A. A. Moiseev^{21,35}, C. Monte^{15,16}, M. E. Monzani⁴, A. Morselli⁴⁵,
I. V. Moskalenko⁴, S. Murgia⁴, T. Nakamori³⁹, P. L. Nolan⁴, J. P. Norris⁴⁶, E. Nuss²⁴,
T. Ohsugi³⁴, A. Okumura⁴², N. Omodei⁵, E. Orlando⁴⁷, J. F. Ormes⁴⁶, D. Paneque⁴,
D. Parent^{32,33}, V. Pelassa²⁴, M. Pepe^{13,14}, M. Pesce-Rollins⁵, F. Piron²⁴, T. A. Porter³¹,
S. Rainò^{15,16}, R. Rando^{10,11}, M. Razzano⁵, A. Reimer^{48,4}, O. Reimer^{48,4}, T. Reposeur^{32,33},
S. Ritz³¹, A. Y. Rodriguez⁴⁹, R. W. Romani⁴, M. Roth¹⁸, F. Ryde^{38,27},
H. F.-W. Sadrozinski³¹, D. Sanchez¹⁷, A. Sander¹², P. M. Saz Parkinson³¹, J. D. Scargle⁵⁰,
T. L. Schalk³¹, C. Sgrò⁵, E. J. Siskind⁵¹, D. A. Smith^{32,33}, P. D. Smith¹², G. Spandre⁵,
P. Spinelli^{15,16}, M. S. Strickman², D. J. Suson⁵², H. Tajima^{4,1}, H. Takahashi³⁴,
T. Takahashi⁴¹, T. Tanaka^{4,1}, J. B. Thayer⁴, J. G. Thayer⁴, D. J. Thompson²⁰,
L. Tibaldo^{10,6,11}, O. Tibolla⁵³, D. F. Torres^{54,49}, G. Tosti^{13,14}, A. Tramacere^{4,55},
Y. Uchiyama^{41,4,1}, T. L. Usher⁴, V. Vasileiou^{20,21,22}, C. Venter^{20,56}, N. Vilchez⁴⁴,
V. Vitale^{45,57}, A. P. Waite⁴, P. Wang⁴, B. L. Winer¹², K. S. Wood², R. Yamazaki³⁴,
T. Ylinen^{38,58,27}, M. Ziegler³¹

¹Corresponding authors: Y. Uchiyama, uchiyama@slac.stanford.edu; S. Funk, funk@slac.stanford.edu; H. Tajima, htajima@slac.stanford.edu; T. Tanaka, ttanaka@slac.stanford.edu.

²Space Science Division, Naval Research Laboratory, Washington, DC 20375, USA

³National Research Council Research Associate, National Academy of Sciences, Washington, DC 20001, USA

⁴W. W. Hansen Experimental Physics Laboratory, Kavli Institute for Particle Astrophysics and Cosmology, Department of Physics and SLAC National Accelerator Laboratory, Stanford University, Stanford, CA 94305, USA

⁵Istituto Nazionale di Fisica Nucleare, Sezione di Pisa, I-56127 Pisa, Italy

⁶Laboratoire AIM, CEA-IRFU/CNRS/Université Paris Diderot, Service d’Astrophysique, CEA Saclay, 91191 Gif sur Yvette, France

⁷Istituto Nazionale di Fisica Nucleare, Sezione di Trieste, I-34127 Trieste, Italy

⁸Dipartimento di Fisica, Università di Trieste, I-34127 Trieste, Italy

⁹Rice University, Department of Physics and Astronomy, MS-108, P. O. Box 1892, Houston, TX 77251, USA

¹⁰Istituto Nazionale di Fisica Nucleare, Sezione di Padova, I-35131 Padova, Italy

¹¹Dipartimento di Fisica “G. Galilei”, Università di Padova, I-35131 Padova, Italy

¹²Department of Physics, Center for Cosmology and Astro-Particle Physics, The Ohio State University, Columbus, OH 43210, USA

¹³Istituto Nazionale di Fisica Nucleare, Sezione di Perugia, I-06123 Perugia, Italy

¹⁴Dipartimento di Fisica, Università degli Studi di Perugia, I-06123 Perugia, Italy

¹⁵Dipartimento di Fisica “M. Merlin” dell’Università e del Politecnico di Bari, I-70126 Bari, Italy

¹⁶Istituto Nazionale di Fisica Nucleare, Sezione di Bari, 70126 Bari, Italy

¹⁷Laboratoire Leprince-Ringuet, École polytechnique, CNRS/IN2P3, Palaiseau, France

¹⁸Department of Physics, University of Washington, Seattle, WA 98195-1560, USA

¹⁹INAF-Istituto di Astrofisica Spaziale e Fisica Cosmica, I-20133 Milano, Italy

²⁰NASA Goddard Space Flight Center, Greenbelt, MD 20771, USA

²¹Center for Research and Exploration in Space Science and Technology (CRESST), NASA Goddard Space Flight Center, Greenbelt, MD 20771, USA

²²University of Maryland, Baltimore County, Baltimore, MD 21250, USA

²³George Mason University, Fairfax, VA 22030, USA

²⁴Laboratoire de Physique Théorique et Astroparticules, Université Montpellier 2, CNRS/IN2P3, Mont-

pellier, France

²⁵Department of Physics and Astronomy, Sonoma State University, Rohnert Park, CA 94928-3609, USA

²⁶Department of Physics, Stockholm University, AlbaNova, SE-106 91 Stockholm, Sweden

²⁷The Oskar Klein Centre for Cosmoparticle Physics, AlbaNova, SE-106 91 Stockholm, Sweden

²⁸Royal Swedish Academy of Sciences Research Fellow, funded by a grant from the K. A. Wallenberg Foundation

²⁹Agenzia Spaziale Italiana (ASI) Science Data Center, I-00044 Frascati (Roma), Italy

³⁰Dipartimento di Fisica, Università di Udine and Istituto Nazionale di Fisica Nucleare, Sezione di Trieste, Gruppo Collegato di Udine, I-33100 Udine, Italy

³¹Santa Cruz Institute for Particle Physics, Department of Physics and Department of Astronomy and Astrophysics, University of California at Santa Cruz, Santa Cruz, CA 95064, USA

³²Université de Bordeaux, Centre d'Études Nucléaires Bordeaux Gradignan, UMR 5797, Gradignan, 33175, France

³³CNRS/IN2P3, Centre d'Études Nucléaires Bordeaux Gradignan, UMR 5797, Gradignan, 33175, France

³⁴Department of Physical Sciences, Hiroshima University, Higashi-Hiroshima, Hiroshima 739-8526, Japan

³⁵University of Maryland, College Park, MD 20742, USA

³⁶Istituto Nazionale di Fisica Nucleare, Sezione di Trieste, and Università di Trieste, I-34127 Trieste, Italy

³⁷University of Alabama in Huntsville, Huntsville, AL 35899, USA

³⁸Department of Physics, Royal Institute of Technology (KTH), AlbaNova, SE-106 91 Stockholm, Sweden

³⁹Department of Physics, Tokyo Institute of Technology, Meguro City, Tokyo 152-8551, Japan

⁴⁰Waseda University, 1-104 Totsukamachi, Shinjuku-ku, Tokyo, 169-8050, Japan

⁴¹Institute of Space and Astronautical Science, JAXA, 3-1-1 Yoshinodai, Sagamihara, Kanagawa 229-8510, Japan

⁴²Department of Physics, Graduate School of Science, University of Tokyo, 7-3-1 Hongo, Bunkyo-ku, Tokyo 113-0033, Japan

⁴³Cosmic Radiation Laboratory, Institute of Physical and Chemical Research (RIKEN), Wako, Saitama 351-0198, Japan

⁴⁴Centre d'Étude Spatiale des Rayonnements, CNRS/UPS, BP 44346, F-30128 Toulouse Cedex 4, France

⁴⁵Istituto Nazionale di Fisica Nucleare, Sezione di Roma "Tor Vergata", I-00133 Roma, Italy

⁴⁶Department of Physics and Astronomy, University of Denver, Denver, CO 80208, USA

⁴⁷Max-Planck Institut für extraterrestrische Physik, 85748 Garching, Germany

⁴⁸Institut für Astro- und Teilchenphysik and Institut für Theoretische Physik, Leopold-Franzens-

ABSTRACT

The discovery of bright gamma-ray emission coincident with supernova remnant (SNR) W51C is reported using the Large Area Telescope (LAT) on board the Fermi Gamma-ray Space Telescope. W51C is a middle-aged remnant ($\sim 10^4$ yr) with intense radio synchrotron emission in its shell and known to be interacting with a molecular cloud. The gamma-ray emission is spatially extended, broadly consistent with the radio and X-ray extent of SNR W51C. The energy spectrum in the 0.2–50 GeV band exhibits steepening toward high energies. The luminosity is greater than 1×10^{36} erg s $^{-1}$ given the distance constraint of $D > 5.5$ kpc, which makes this object one of the most luminous gamma-ray sources in our Galaxy. The observed gamma-rays can be explained reasonably by a combination of efficient acceleration of nuclear cosmic rays at supernova shocks and shock-cloud interactions. The decay of neutral π -mesons produced in hadronic collisions provides a plausible explanation for the gamma-ray emission. The product of the average gas density and the total energy content of the accelerated protons amounts to $\bar{n}_H W_p \simeq 5 \times 10^{51} (D/6 \text{ kpc})^2$ erg cm $^{-3}$. Electron density constraints from the radio and X-ray bands render it difficult to explain the LAT signal as due to inverse Compton scattering. The *Fermi* LAT source coincident with SNR W51C sheds new light on the origin of Galactic cosmic rays.

Subject headings: acceleration of particles — ISM: individual(W51C) — radiation mechanisms: non-thermal

Universität Innsbruck, A-6020 Innsbruck, Austria

⁴⁹Institut de Ciències de l'Espai (IEEC-CSIC), Campus UAB, 08193 Barcelona, Spain

⁵⁰Space Sciences Division, NASA Ames Research Center, Moffett Field, CA 94035-1000, USA

⁵¹NYCB Real-Time Computing Inc., Lattingtown, NY 11560-1025, USA

⁵²Department of Chemistry and Physics, Purdue University Calumet, Hammond, IN 46323-2094, USA

⁵³Max-Planck-Institut für Kernphysik, D-69029 Heidelberg, Germany

⁵⁴Institució Catalana de Recerca i Estudis Avançats, Barcelona, Spain

⁵⁵Consorzio Interuniversitario per la Fisica Spaziale (CIFS), I-10133 Torino, Italy

⁵⁶North-West University, Potchefstroom Campus, Potchefstroom 2520, South Africa

⁵⁷Dipartimento di Fisica, Università di Roma “Tor Vergata”, I-00133 Roma, Italy

⁵⁸School of Pure and Applied Natural Sciences, University of Kalmar, SE-391 82 Kalmar, Sweden

1. Introduction

The origin of cosmic rays remains unsolved. The idea that supernovae produce cosmic rays (e.g., Hayakawa 1956) has been developed both in theoretical and observational aspects, so that galactic cosmic rays are widely considered to be accelerated in the expanding shocks of supernova remnants (SNRs) through diffusive shock acceleration process (see e.g., Blandford & Eichler 1987). This conjecture has been strengthened by recent observations of young SNRs in synchrotron X-rays and very-high-energy (VHE) gamma-rays (see e.g., Reynolds 2008; Aharonian et al. 2008). High efficiency for converting the kinetic energy released by supernova explosions into the energy of relativistic protons and nuclei is a key requirement to explain the galactic cosmic rays; it is yet to be confirmed observationally.

Enhanced π^0 -decay emission expected from SNRs that are interacting with molecular clouds could provide direct evidence of the nuclear component of cosmic rays being accelerated at supernova shocks (Aharonian et al. 1994). To identify the π^0 -decay gamma-rays as evidence of the nuclear cosmic rays, observations in the GeV domain are crucial because the π^0 -decay spectrum has a characteristic bump around 70 MeV. Previous measurements of GeV gamma-rays with EGRET onboard the Compton Gamma-Ray Observatory found some gamma-ray sources near radio-bright SNRs (Esposito et al. 1996). However, the possible origins of the EGRET sources, namely SNR shell contributions or pulsar associations, remained unclear, mainly due to poor localization.

The advent of the Large Area Telescope (LAT) onboard the *Fermi* Gamma-ray Space Telescope provides a new opportunity to study the gamma-ray emission from SNRs at GeV energies. An initial source list based on the first three months of *Fermi* observations (Abdo et al. 2009c) includes 0FGL J1923.0+1411, which is spatially coincident with SNR W51C. Even with the three months data, the detection was at $\sim 23\sigma$ level. There are no EGRET counterpart(s) to the LAT source (Hartman et al. 1999); this is the first SNR discovered by *Fermi* as confirmed in this paper.

W51C (G49.2–0.7) is a radio-bright SNR at a distance of $D \simeq 6$ kpc with an estimated age of $\sim 3 \times 10^4$ yrs (Koo et al. 1995). It has an elliptical shape with an extent of $50' \times 38'$. The radio continuum map exhibits thick shell-like structures (Subrahmanyan & Goss 1995). The bulk of the X-ray emission comes from thermal plasma with a temperature of $kT \sim 0.3$ keV (Koo et al. 2005). A molecular cloud–shock interaction is known, as evidenced by observations of shocked atomic and molecular gases (Koo & Moon 1997a,b). Most recently, the HESS collaboration has announced the detection of extended VHE gamma-ray emission coincident with W51C (Fiasson et al. 2009). Also, the Milagro collaboration has reported a possible excess of multi-TeV gamma-rays in this direction (Abdo et al. 2009a).

In this paper we report the analysis results for the LAT source coincident with SNR W51C, using data accumulated over the first year of *Fermi*'s operation. The *Fermi* observations of SNR W51C permit a refined study of cosmic-ray acceleration. Specifically, the LAT data suggest that π^0 -decay emission is the dominant contribution to the gamma-ray signal.

2. Observation and Data Reduction

The *Fermi* Gamma-ray Space Telescope was launched on 2008 June 11 by a Delta II Heavy launch vehicle. The LAT onboard *Fermi* is a pair-conversion gamma-ray detector capable of measuring gamma-rays in a very wide range of energy from 20 MeV up to 300 GeV. The LAT tracks the electron and positron resulting from pair conversion of an incident gamma-ray in thin high- Z foils, and measures the energy deposition due to the subsequent electromagnetic shower that develops in the calorimeter. The effective area is ~ 8000 cm² above 1 GeV (on-axis) and the per-photon 68% containment radius is ~ 0.8 at 1 GeV. The point-spread function (PSF) depends largely on photon energy and improves at higher energies. The tracker of the LAT is divided into two regions, *front* and *back*. The front region (first 12 planes) has thin converters to optimize the PSF while the back region (4 planes after the front section) has thicker converters to enlarge the effective area. The angular resolution for the back events is approximately twice as broad than that for the front events. The details of the LAT and data processing are given in Atwood et al. (2009), and the on-orbit calibration is described in Abdo et al. (2009b).

The gamma-ray data acquired from 2008 August 5 to 2009 July 14 are analyzed. The *diffuse* class events as defined in Atwood et al. (2009) are chosen for gamma-ray analysis. A cut on earth zenith angles greater than 105° is applied to reduce the residual signal from earth albedo gamma-rays. The instrument response functions (IRFs) called “Pass 6 V3” are used (Rando et al. 2009).

3. Analysis and Results

The maximum likelihood technique is employed for spectral and spatial parameter estimation using *gtlike*, which is publicly available as part of *Fermi* Science Tools¹. The likelihood is the product of the probability of observing the gamma-ray counts of each spatial

¹Software and documentation of the *Fermi* Science Tools are distributed by the Fermi Science Support Center at <http://fermi.gsfc.nasa.gov/ssc>

and energy bin given the emission model, and parameter values are estimated by maximizing the likelihood of the data given the model (Mattox et al. 1996). The gamma-ray emission model includes individual sources at fixed coordinates, galactic diffuse emission (resulting from cosmic-ray interactions with interstellar gas and photons), and an isotropic component (extragalactic and residual background). The so-called “mapcube” file of `gll_iem_v02.fit` is used for modeling the galactic diffuse emission, together with the corresponding tabulated model for the isotropic diffuse emission. Other versions of the galactic diffuse models, generated by the GALPROP code (Strong et al. 2004), are also utilized to assess systematic error. The maximum likelihood analysis is performed inside a square region of $12^\circ \times 12^\circ$ centered on W51C with a pixel size of $0^\circ.1$, unless otherwise mentioned. Background point sources detected in six months data are included in the likelihood analysis with free normalization and power-law index, though none of them affect the results in this paper.

3.1. Spatial Distribution

In Figure 1, the maps of photon counts in the 2–10 GeV band in the vicinity of SNR W51C are shown; the right panel is a close-up view of the left panel. Gamma-ray events that converted in the *front* section of the tracker are selected. A bright gamma-ray source is enclosed by the outer boundary of W51C. The average surface brightness inside the SNR boundary is about 2 and 5 times larger than neighboring regions on the galactic plane in the 0.5–2 GeV and 2–10 GeV bands, respectively. The gamma-ray distribution appears to be somewhat clumpy, suggesting the presence of sub-structures. Due to the limited statistics, we defer the investigation of possible sub-structures to a future publication.

The spatial distribution of the gamma-ray source is significantly extended compared to a simulated point source that has the same spectrum. A one dimensional profile in the right ascension direction of the counts map is compared with that expected for a point source in Figure 2. Though the width of the PSF above 5 GeV is known to deviate from the Monte Carlo simulations, it has negligible effects on the simulated point source and other results in this paper. Assuming a two-dimensional gaussian distribution fixed at the W51C centroid $(\alpha, \delta) = (290^\circ.818, 14^\circ.145)$, we calculate the extension parameter of the source as $\sigma_{\text{ext}} = 0^\circ.22 \pm 0^\circ.02$ by varying σ_{ext} to find the best match with the data. Note however that a different assumption on the spatial distribution results in different quantification of the spatial extension.

The extended nature of this LAT source cannot be ascribed to a superposition of two point-like sources. To quantify this, we define a grid of 60 positions inside the remnant as trial point source positions, and calculate maximum likelihood values ($L_{2\text{ps}}$) for each

possible combination by running *gtlike* for a box of $8^\circ \times 8^\circ$. On the other hand, assuming that the gamma-ray source has uniform surface brightness inside the SNR boundary, we obtain another maximum likelihood value (L_{uni}). The resulting values of the likelihood test statistics, $-2 \ln(L_{2\text{ps}}/L_{\text{uni}}) > 32$, demonstrate that the uniform emission gives a much better result.

The extension of the source precludes magnetospheric radiation from a pulsar as a dominant gamma-ray source. However, a small fraction ($\sim 10\%$) of the gamma-ray flux could be contributed by a pulsar. Our pulse search results in non-detection, which places a 5σ upper limit on the pulsed gamma-rays as $\simeq 6 \times 10^{-8}$ photons $\text{cm}^{-2} \text{s}^{-1}$ above 100 MeV (see Abdo et al. 2009d).

3.2. Spectrum and Its Uncertainties

The gamma-ray spectrum of the W51C source is shown in Figure 3. It is obtained by performing likelihood analysis for each energy bin with *gtlike*. The lower energy bound is set at 0.2 GeV, below which the systematic uncertainties become too large due to the background diffuse emission (see below). The surface brightness of the W51C source is assumed to be uniform inside the SNR boundary. The normalization of the galactic diffuse emission model is left free at each energy bin. As evident from Figure 3, the gamma-ray spectrum cannot be described by a simple power law and steepens above a few GeV. A likelihood-ratio test indicates that a power-law hypothesis has a chance probability of 5×10^{-5} for obtaining the spectral data. The physical interpretation of the spectral energy distribution will be discussed in §4.

The gamma-ray luminosity can be estimated as $\simeq 1 \times 10^{36} (D/6 \text{ kpc})^2 \text{ erg s}^{-1}$ in the LAT bandpass, making this object one of the most luminous gamma-ray sources in our Galaxy. Note that the distance to the remnant is well constrained. X-ray absorption (Koo et al. 1995) indicates that W51C is situated behind the W51 molecular cloud complex (a so-called 68 km s^{-1} cloud in particular) whose distance is determined as $7.0 \pm 1.5 \text{ kpc}$ by the proper motion of W51 Main H_2O maser (Genzel et al. 1981). On the other hand, the angular extent and the X-ray measurements (Koo et al. 2002) require $D \lesssim 10 \text{ kpc}$. We adopt $D = 6 \text{ kpc}$ following previous publications (e.g., Koo et al. 2005).

It should be noted that in addition to the systematic errors commonly assigned to LAT spectral data², the accuracy of the flux estimated for each energy bin of the W51C source

²For the IRF used here (P6_V3_DIFFUSE), systematic error as a function of $x = \log(E/\text{MeV})$ is 10% at

is limited by the following errors. First, a possible effect of the uncertainty of underlying galactic diffuse emission is considered. The observed gamma-ray intensity of nearby source-free regions on the galactic plane is compared with the intensity expected from the galactic diffuse models. The difference, namely the local departure from the best-fit diffuse model, is found to be $\lesssim 6\%$. By changing the normalization of the galactic diffuse model artificially by $\pm 6\%$, we estimate the possible systematic error to be 40% (0.2–0.4 GeV), 22% (0.4–0.8 GeV) and $< 10\%$ (> 0.8 GeV).

The fact that we do not know the true gamma-ray morphology of the W51C source introduces another error in our flux estimation. Since the gamma-ray source is point-like below 1 GeV given the PSF, this uncertainty matters only above 1 GeV. We adopt a uniform surface brightness inside the SNR boundary (a flat elliptical template) as the spatial distribution of the source gamma-rays. Different spatial distributions such as a flat elliptical template reduced in size (scaled by 0.5) are tested to estimate the systematic error. Our conservative estimate is $\lesssim 20\%$ in 1–6 GeV and $\sim 30\%$ above 6 GeV as the systematic uncertainty attributable to the unknown shape of the source.

4. Discussion

The extended gamma-ray emission positionally coincident with SNR W51C has been studied using the *Fermi* LAT. The gamma-ray spectrum presented in Figure 3 is not fit by a simple power law, exhibiting a remarkable steepening. Here we discuss the origin of the extended emission and the underlying particle spectra that give rise to the observed spectrum of photons.

The expanding shock waves driven by the supernova explosion are expected to be the sites of the acceleration of multi-GeV particles. To phenomenologically interpret the spectral curvature in the LAT+TeV bands, a broken power-law is adopted for the momentum distribution of the radiating electrons/protons:

$$N_{e,p}(p) = a_{e,p} \left(\frac{p}{p_0} \right)^{-s} \left(1 + \left(\frac{p}{p_{\text{br}}} \right)^2 \right)^{-\Delta s/2}, \quad (1)$$

where $p_0 = 1 \text{ GeV } c^{-1}$. For simplicity, the indices and the break momentum are assumed to be identical for both accelerated protons and electrons. As we argue below, the break may reflect the character of magnetohydrodynamic turbulence. To account for the radio synchrotron

$x = 2$, 5% at $x = 2.75$, and 20% at $x = 4$ with a linear interpolation between them.

index $\alpha \simeq 0.26$ (Moon & Koo 1994), we adopt $s = 1.5$, though a steeper index (say, $s = 1.7$) could be reconciled with the radio observations within the uncertainty. The energetic particles are assumed to be uniformly distributed in the volume of $V = (4\pi/3)R_{\text{eff}}^3$ with an effective radius $R_{\text{eff}} = 30$ pc. The age and radius imply a shock velocity of $v_{\text{sh}} \sim 400$ km s $^{-1}$ and $E_{\text{SN}}/n_0 \sim 1.6 \times 10^{52}$ erg cm 3 , where E_{SN} and n_0 represent the explosion kinetic energy and the interstellar density into which the main blast wave is propagating, respectively. The X-ray data suggest $n_0 \sim 0.3$ cm $^{-3}$. The radio images indicate that radio-emitting electrons are smoothly distributed in a thick shell. The model of Koo & Moon (1997a) suggests the presence of a molecular cloud of $\sim 1 \times 10^4 M_{\odot}$ engulfed by the blast wave. The engulfed cloud can act as target material for relativistic particles. The total (atomic and molecular) hydrogen mass contained in the volume is denoted by $M_{\text{H}} = \bar{n}_{\text{H}}m_pV$. Note that $\bar{n}_{\text{H}} \gg n_0$ can be expected.

Given the interaction with a molecular cloud, we first attribute the observed gamma-rays to the decay of π^0 mesons produced in inelastic collisions between accelerated protons (and nuclei) and target gas (Fig. 3). The gamma-ray spectrum of π^0 -decay is calculated based on Kamae et al. (2006) using a scaling factor of 1.85 for helium and heavy nuclei (Mori 2009). Note that the scaling factor assumes the local interstellar abundance for target material and the observed cosmic-ray composition. Contributions from bremsstrahlung and Inverse-Compton (IC) scattering by accelerated electrons are also shown in Fig. 3. Electron-ion and electron-electron bremsstrahlung spectra are computed as in Baring et al. (1999). The interstellar radiation field for IC (see Table 1) is comprised of two diluted blackbody components (infrared and optical) and the CMB. The infrared and optical components are adjusted to reproduce the interstellar radiation field in the GALPROP code (Porter et al. 2008). Cooling effects due to ionization and synchrotron (or IC) losses, which introduce cooling breaks in particle spectra in addition to p_{br} , are taken into account assuming constant particle injection over a period $T_0 \sim 3 \times 10^4$ yr. The synchrotron cooling becomes important in the TeV band for leptonic models.

Figure 4 (a) shows the radio+gamma-ray spectrum together with the radiation model that uses the parameters in Table 1. We adopt here $M_{\text{H}} = 2.8 \times 10^4 M_{\odot}$ ($\bar{n}_{\text{H}} = 10$ cm $^{-3}$), which is somewhat larger than the value quoted above. The total energy of the high-energy protons amounts to $W_p = 5.2 \times 10^{50}$ erg, which is inversely proportional to M_{H} , but insensitive to other parameters. The large luminosity of the LAT source can be explained naturally by a large number of accelerated protons and dense environments as expected for the case of W51C.

The break feature in the proton spectrum, which is introduced on phenomenological grounds, is not expected in a shock acceleration zone if acceleration proceeds close to the

Bohm limit (e.g., Baring et al. 1999). Protons can be accelerated up to ~ 200 TeV via diffusive shock acceleration with a power-law (or even slightly concave) momentum distribution. A possible explanation for the falling proton spectrum above $p_{\text{br}} = 10\text{--}30 \text{ GeV } c^{-1}$ (which depends on the choice of other parameters) could be the effects of damping of magnetohydrodynamic turbulence due to ion-neutral collisions. According to Ptuskin & Zirakashvili (2003), the maximum attainable momentum in the presence of wave dissipation by ion-neutral collisions is estimated as $p_{\text{max}}(T_0) \sim 30 (n/1 \text{ cm}^{-3})^{-1/2} \text{ GeV } c^{-1}$, using the SNR parameters described above. Here n is the ambient neutral gas density. The shock precursor cannot confine accelerated protons with $p > p_{\text{max}}(T_0)$ even if they were accelerated earlier. Therefore, energy-dependent escape of accelerated particles from the remnant (e.g., Aharonian & Atoyan 1996) may account for the steepening of the proton distribution. In any case, a break is needed to fit the observed SED.

In contrast, leptonic models for the GeV gamma-ray production face difficulties (see Figure 4b–c and Table 1). While the chosen model parameters are not unique in their ability to fit the broadband spectrum, they are representative; no reasonable choices for them can easily account for the radio+gamma-ray data. Leptonic scenarios require a_e/a_p far in excess of cosmic-ray abundance ratios. It is difficult to reconcile the bremsstrahlung-dominated model with the observed radio synchrotron spectrum (Fig. 4b). Also, the IC-dominated model (Fig. 4c) requires an unrealistically large energy content in radiating electrons, $W_e \simeq 1 \times 10^{51}$ erg, a low magnetic field of $B \simeq 2 \mu\text{G}$ (to suppress the radio synchrotron emission), and a low density of $\bar{n}_{\text{H}} < 0.1 \text{ cm}^{-3}$ (to reduce the bremsstrahlung component). Such a low density is problematic because even X-ray-emitting gas has a density of $\sim 1 \text{ cm}^{-3}$ (Koo et al. 2002). It is also difficult to account for the LAT signal by an IC process in a possible pulsar wind nebula seen inside W51C, CXO J192318.5+143035 (Koo et al. 2005), which has only a few parsec extent and much weaker radio emission compared with the SNR shell.

The most plausible explanation for the LAT source is therefore offered by π^0 -decay gamma-rays in a dense environment, spawned by efficient acceleration of protons and nuclei taking place or having taken place at the shocked shell of SNR W51C. The discovery of the GeV-scale gamma-rays presented in this paper raises the intriguing possibility that *Fermi* has discerned accelerated ions in a middle-aged remnant that is interacting with dense clouds.

The *Fermi* LAT Collaboration acknowledges support from a number of agencies and institutes for both development and the operation of the LAT as well as scientific data analysis. These include NASA and DOE in the United States, CEA/Irfu and IN2P3/CNRS in France, ASI and INFN in Italy, MEXT, KEK, and JAXA in Japan, and the K. A. Wallenberg Foundation, the Swedish Research Council and the National Space Board in Sweden. Additional support from INAF in Italy and CNES in France for science analysis during the

operations phase is also gratefully acknowledged.

REFERENCES

- Abdo, A. A., et al. (the Milagro collaboration), 2009a, *ApJ*, 700, L127
- Abdo, A. A., et al. (the Fermi LAT collaboration), 2009b, *Astroparticle Physics* in press, arXiv:0904.2226
- Abdo, A. A., et al. (the Fermi LAT collaboration), 2009c, *ApJS*, 183, 46
- Abdo, A. A., et al. (the Fermi LAT collaboration), 2009d, submitted to *ApJ*
- Aharonian, F. A., & Atoyan, A. M. 1996, *A&A*, 309, 917
- Aharonian, F., Buckley, J., Kifune, T., & Sinnis, G. 2008, *Reports on Progress in Physics*, 71, 096901
- Aharonian, F. A., Drury, L. O., & Völk, H. J. 1994, *A&A*, 285, 645
- Atwood, W. B., et al. (the Fermi LAT collaboration), 2009, *ApJ*, 697, 1071
- Baring, M. G., Ellison, D. C., Reynolds, S. P., Grenier, I. A., & Goret, P. 1999, *ApJ*, 513, 311
- Blandford, R., & Eichler, D. 1987, *Phys. Rep.*, 154, 1
- Carpenter, J. M., & Sanders, D. B. 1998, *AJ*, 116, 1856
- Esposito, J. A., Hunter, S. D., Kanbach, G., & Sreekumar, P. 1996, *ApJ*, 461, 820
- Fiasson, A., Marandon, V., Chaves, R. C. G., & Tibolla, O. (the HESS collaboration), 2009, in the proceedings of the 31st International Cosmic Ray Conference
- Genzel, R., et al. 1981, *ApJ*, 247, 1039
- Hartman, R. C., et al. 1999, *ApJS*, 123, 79
- Hayakawa, S. 1956, *Progress of Theoretical Physics*, 15, 111
- Kamae, T., Karlsson, N., Mizuno, T., Abe, T., & Koi, T. 2006, *ApJ*, 647, 692
- Koo, B.-C., Kim, K.-T., & Seward, F. D. 1995, *ApJ*, 447, 211

- Koo, B.-C., Lee, J.-J., & Seward, F. D. 2002, *AJ*, 123, 1629
- Koo, B.-C., Lee, J.-J., Seward, F. D., & Moon, D.-S. 2005, *ApJ*, 633, 946
- Koo, B.-C., & Moon, D.-S. 1997a, *ApJ*, 475, 194
- Koo, B.-C., & Moon, D.-S. 1997b, *ApJ*, 485, 263
- Mattox, J. R., et al. 1996, *ApJ*, 461, 396
- Moon, D.-S., & Koo, B.-C. 1994, *Journal of Korean Astronomical Society*, 27, 81
- Mori, M. 2009, *Astroparticle Physics*, 31, 341
- Porter, T., et al. 2008, *ApJ*, 682, 400
- Ptuskin, V. S., & Zirakashvili, V. N. 2003, *A&A*, 403, 1
- Rando, R., et al. (the Fermi LAT collaboration), 2009, in the proceedings of the 31st International Cosmic Ray Conference, (arXiv:0907.0626)
- Reynolds, S. P. 2008, *ARAA*, 46, 89
- Strong, A. W., Moskalenko, I. V., & Reimer, O. 2004, *ApJ*, 613, 962
- Subrahmanyan, R., & Goss, W. M. 1995, *MNRAS*, 275, 755

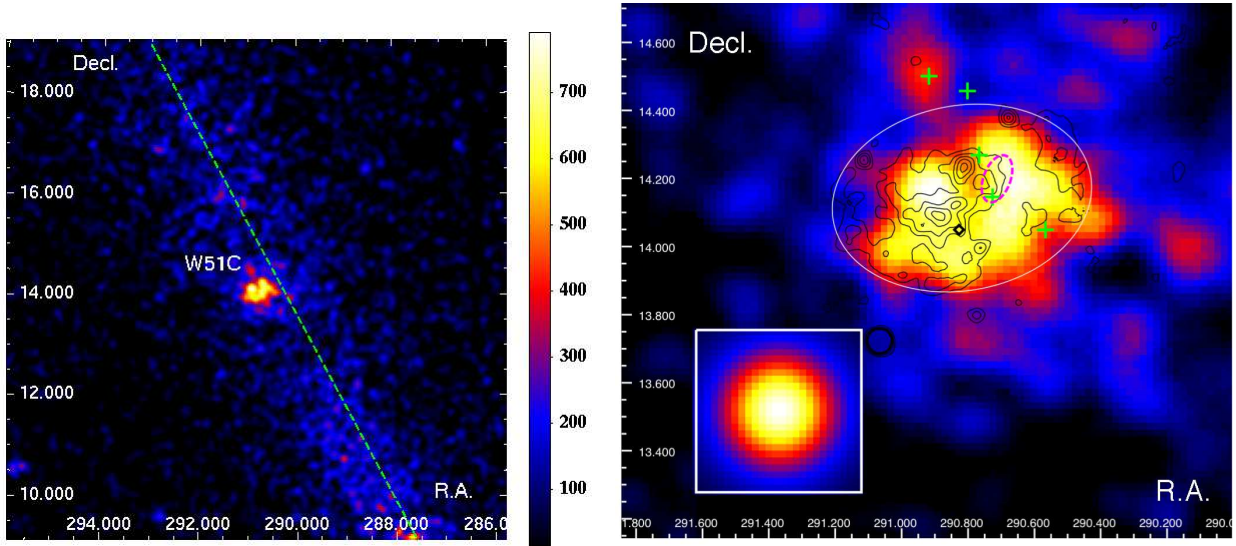


Fig. 1.— (Left) *Fermi* LAT counts map in 2–10 GeV around SNR W51C in units of counts per deg². Front-converted events are selected. The counts map is smoothed by a Gaussian kernel of $\sigma = 0\text{.}12$. The green dashed line represents the galactic plane. (Right) Close up view around SNR W51C. The simulated point source image (smoothed by the same gaussian) is shown in the inset. The outer boundary of W51C is indicated by a white ellipse. Superposed is the ROSAT X-ray map (contours) from Koo et al. (1995). The region where shocked CO clumps (Koo & Moon 1997b) were found is represented by a dashed magenta ellipse. A diamond near the SNR centroid indicates CXO J192318.5+143035 (see the text). The positions of five HII regions are indicated by green crosses (Carpenter & Sanders 1998).

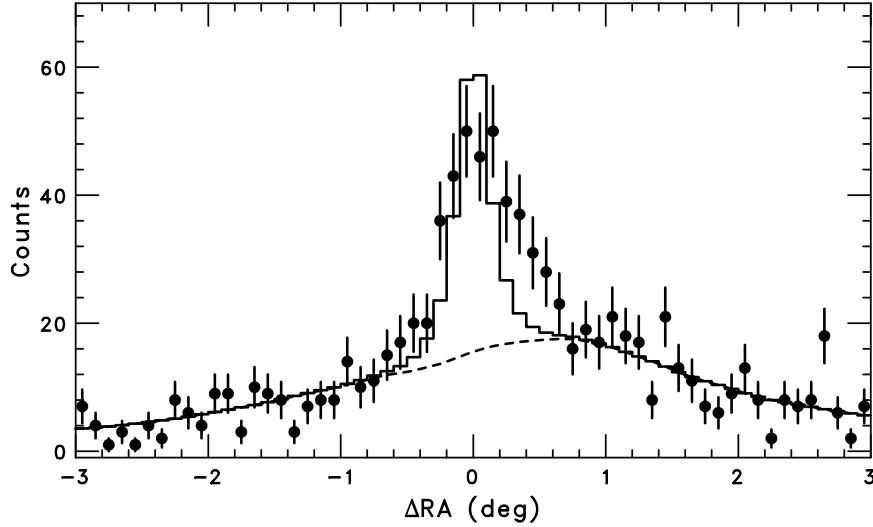


Fig. 2.— One dimensional profile of the observed 2–10 GeV gamma-rays (data points) along right ascension. The counts map is integrated over the direction of declination with a width of $\Delta\delta = 1.6$ centered on W51C. The dashed curve shows the profile of the galactic+isotropic diffuse model. The histogram represents the sum of a simulated point source and the diffuse model.

Table 1. Parameters of Multiwavelength Models

Model	Parameters					Energetics	
	a_e/a_p	Δs	p_{br} (GeV c^{-1})	B (μG)	\bar{n}_{H} (cm^{-3})	W_p (10^{50} erg)	W_e (10^{50} erg)
(a) π^0 -decay	0.02	1.4	15	40	10	5.2	0.13
(b) Bremsstrahlung	1.0	1.4	5	15	10	0.54	0.87
(c) Inverse Compton	1.0	2.3	20	2	0.1	8.4	11

Note. — Seed photons for IC include the CMB ($kT_{\text{CMB}} = 2.3 \times 10^{-4}$ eV, $U_{\text{CMB}} = 0.26$ eV cm^{-3}), infrared ($kT_{\text{IR}} = 3 \times 10^{-3}$ eV, $U_{\text{IR}} = 0.90$ eV cm^{-3}), and optical ($kT_{\text{opt}} = 0.25$ eV, $U_{\text{opt}} = 0.84$ eV cm^{-3}). The total energy content of radiating particles, $W_{e,p}$, is calculated for $p > 10$ MeV c^{-1} .

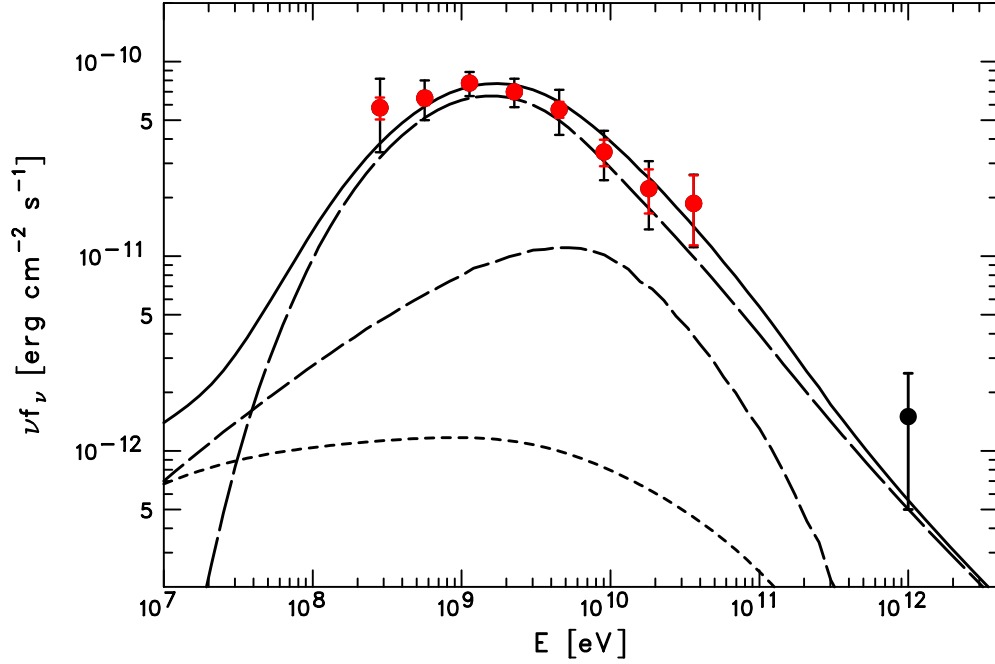


Fig. 3.— SED of the SNR W51C region measured with the *Fermi* LAT (red points) together with phenomenological modeling. Systematic errors (see §3.2) are indicated by black bars. The model consists of π^0 -decay (long-dashed curve), bremsstrahlung (dashed curve), and IC scattering (short-dashed curve). The integrated flux reported by HESS is converted to the differential flux at 1 TeV assuming photon index $\Gamma = 2.5 \pm 1.0$ (black point).

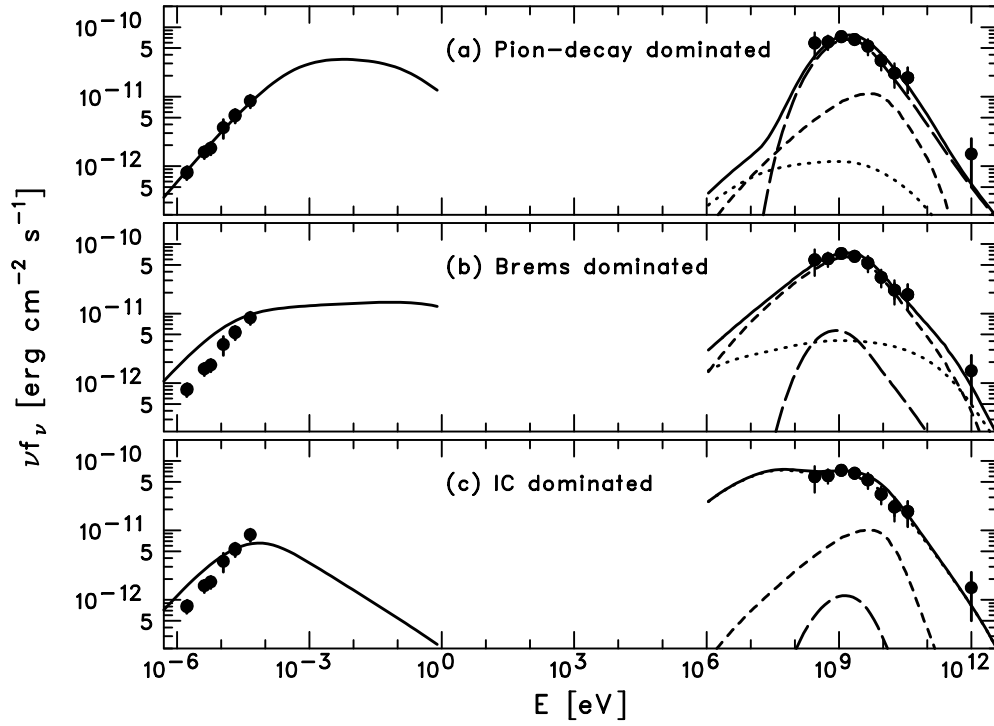


Fig. 4.— Three different scenarios for the multiwavelength modeling (see Table 1). The radio emission (from Moon & Koo 1994) is explained by synchrotron radiation, while the gamma-ray emission is modeled by different combinations of π^0 -decay (long-dashed curve), bremsstrahlung (dashed curve), and IC scattering (dotted curve). The sum of the three component is shown as a solid curve.